Dynamic Covalent Polypeptides Showing Tunable Secondary Structures and Thermoresponsiveness

Jiatao Yan, Kun Liu, Xiuqiang Zhang, Wen Li, Afang Zhang

Laboratory of Polymer Chemistry, Department of Polymer Materials, College of Materials Science and Engineering, Shanghai University, Nanchen Road 333, Shanghai 200444, China
Correspondence to: A. Zhang (E-mail: azhang@shu.edu.cn)

Received 21 July 2014; accepted 29 September 2014; published online 20 October 2014
DOI: 10.1002/pola.27433

ABSTRACT: Lysine-based polypeptides can be afforded with steerable secondary structures and tunable thermoresponsiveness through dynamic covalent OEGylation. These polypeptides were formed through dynamic imine linkage via reactions of amino moieties from poly(L-lysine)s with aldehydes from oligoethylene glycol (OEG)-based dendrons. In addition to solution concentrations and pH values, macromolecular effect was found to play an important role on the imine formation. OEGylated polypeptides showed characteristic thermoresponsive properties, and their phase transition temperatures were governed predominately by terminal groups and the coverage of OEG dendrons. Notably, thermally induced aggregation would enhance the imine formation even at elevated temperature. In contrast to the covalent polypeptide representatives, the dynamic covalent polypeptides conveyed different thermoresponsiveness due to imine linkages, and their phase transition temperatures could be tuned simply by varying ratios of OEG dendrons with different hydrophilicity. Furthermore, helical conformation of these polypeptides was enhanced with attachment of OEG dendrons, and could be reversibly switched through thermally induced aggregation. © 2014 Wiley Periodicals, Inc. J. Polym. Sci., Part A: Polym. Chem. **2015**, *53*, 33–41

KEYWORDS: dendrimers; dynamic covalent chemistry; helical conformation; peptides; secondary structures; stimuli-sensitive polymers

INTRODUCTION Polypeptides have formed a class of important bio-mimicking polymers, whose ordered secondary structures, such as α-helix and β-sheet, play crucial roles in mediating their biological functions and material applications.[1] The stability of these secondary structures is dominated by the peptide chain length, amino acid sequence, and also architectures.[2] Charges along peptide chains provide water solubility, but always decrease helicity due to coulomb repulsion. Many strategies such as side-chain crosslinking,[3] hydrogen-bond surrogate,[4] metal coordination,[5] salt bridge formation,[6] and self-assembly[7] have been used to modulate the secondary structures of peptides with specific sequences. Alternatively, by elongating the distance between charged pendants and polypeptide backbone, ionic polypeptides were found to show remarkable helical stability against changes in pH, temperature, and denaturing reagents.[8] This structural effect was proposed to be attributable to the decrease of charge repulsion and increase of side-chain hydrophobicity. Recently, much attention has been paid to synthesize stimuli-responsive polypeptides, whose secondary structures or macroscopic properties can be switched by external stimuli such as temperature, pH, and redox.[9] For example, copolypeptides from glutamate and glucosylated allyl- or propargylglycine exhibited characteristic pH-switchable conformations and bioactivity, together with enhanced helicity.[10] Through the responsive thioether linkage, glycosylated poly(*S*-alkyl-L-homocysteine)s underwent redox-triggered helix-to-coil transition.[11] Further studies on stimuli-responsive polypeptides with tunable secondary structures will not only help to understand and control some abnormal conformation transformation related to amyloid-based diseases[12] but also be potentially helpful in designing for drug delivery system, tissue engineering, and smart materials.[13]

Thermoresponsive polypeptides are one of the most attractive stimuli-responsive polypeptides, and have found promising applications in various areas. One intriguing class of thermoresponsive polypeptides are those based on elastin-like polypeptides (ELPs).[14] These polypeptides exhibit reversible thermally induced phase transition behavior in aqueous solutions, accompanying the secondary structure change from random coil to β-spiral. The excellent biocompatibility makes ELPs useful for a wide variety of biomedical applications. However, linear ELPs always show broad-phase

Additional Supporting Information may be found in the online version of this article.

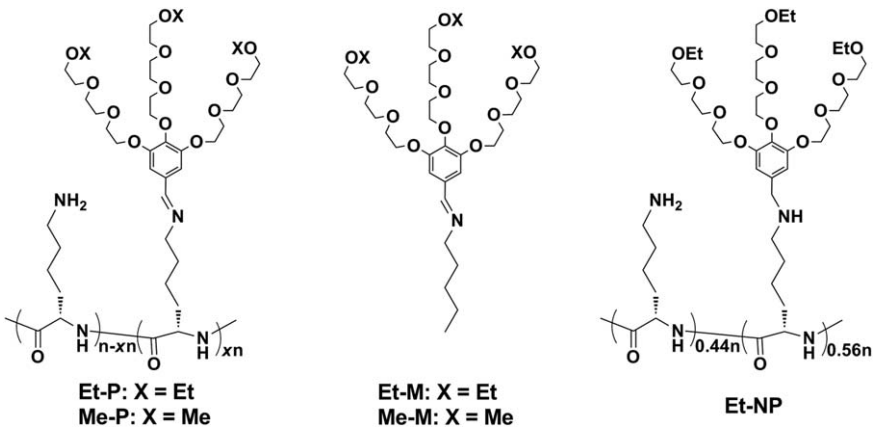

FIGURE 1 Molecular structures of dynamic OEGylated polypeptides (**Et-P**, **Me-P**), monomeric imines (**Et-M**, **Me-M**), and nondynamic OEGylated polypeptide (**Et-NP**) discussed in this work.

transitions and large hysteresis owing to the strong hydrogen bonding from amide moieties. To avoid these, various thermoresponsive polypeptides with different chemical structures or architectures have been developed to mimic ELPs. Oligopeptides or polypeptides can be afforded with thermoresponsive properties through covalent modification to elegantly tune the hydrophilicity–hydrophobicity balance.[15] Oligo (ethylene glycol)s (OEGs) were utilized as motifs to mediate polypeptides with superior thermoresponsiveness. The polypeptides such as poly(L-lysine)s, poly(L-glutamate)s, and poly(L-cysteine)s carrying linear OEG units in their side chains were found to be thermoresponsive, and their phase transition temperatures can be modulated by varying OEG length, ratios of comonomers, and even chirality of polypeptides.[16] Alternatively, polyprolines grafted with bulky OEG dendrons show appealing thermoresponsive behavior, whose thermoresponsive properties and secondary structures are dependent on both dendron generation and arrangement of dendrons along the polypeptide backbones.[17] Despite the great progress in synthetic strategies, most thermoresponsive polypeptides reported to date are constructed through covalent linkage. Their chemical structures or architectures are fixed once the polypeptides were prepared. It is hard to tune their thermoresponsive properties at will without breaking them, and therefore, it remains a challenge to develop novel strategies for preparing thermoresponsive polypeptides with truly tunable phase transition temperatures.

Dynamic covalent chemistry (DCC) relies on the reversible formation and breaking of covalent bonding under thermodynamic control, which has been proven to be a powerful strategy to mediate polymers with responsive and adaptive properties.[18] The dynamic covalent linkages allow the component exchanges and structure reshuffles under certain conditions, which can be kinetically fixed after removal of catalyst.[19] Various reversible covalent linkages, including disulfide, imine, and acylhydrazone, have been consciously selected to construct dynamic covalent (poly)peptides, which show promising applications in synthetic receptors,[20] self-replication,[21] and responsive assembly.[22] However, less attention was paid to afford them with thermoresponsiveness[23] and, at the same time, to switch their secondary structures.[24] To combine thermoresponsive polypeptides with dynamic characteristics, we here present the synthesis of OEGylated polypeptides through DCC (Fig. 1). Dendritic OEG moieties were selected on one side to efficiently shield hydrogen bonding of amide units in polypeptide backbones, and on the other side to provide thermoresponsiveness. These dynamic covalent polypeptides inherit superior thermoresponsive properties from their parent OEG-based dendronized polymers;[25] simultaneously, their thermoresponsiveness and secondary structures can be finely tuned and controlled through the dynamic covalent linkages.

EXPERIMENTAL

Materials

Ethoxyl- and methoxyl-terminated first-generation OEG-based dendritic alcohols were synthesized according to our previous reports.[25(b)] Poly-L-lysine hydrochloride (**PLL**) (molecular weight by viscosity = 48,600) was purchased from Sigma-Aldrich. Buffer solutions were prepared by adding appropriate amounts of NaOH to 30 mM $NaHCO_3$ aqueous solutions, and pH values (11, 10, 9) were calibrated with a Metler Toledo seven compact S220-B pH meter. Dichloromethane (DCM) was dried over CaH_2. Other reagents and solvents were purchased at reagent grade and used without further purification. All reactions were run under a nitrogen atmosphere. Macherey-Nagel precoated TLC plates (silica gel 60 G/UV254, 0.25 mm) were used for thin-layer chromatography (TLC) analysis. Silica gel 60 M (Macherey-Nagel, 0.04–0.063 mm, 200–300 mesh) was used as the stationary phase for column chromatography.

Instrumentation and Measurements

^1H and ^{13}C NMR spectra were recorded on a Bruker AV 500 (^1H: 500 MHz, ^{13}C: 125 MHz) spectrometer. High-resolution MALDI-TOF-MS analyses were performed on IonSpec Ultra instruments. UV/vis turbidity measurements were carried out on a PE UV/vis spectrophotometer Lambda 35 equipped with a thermostatically regulated bath. Sample solutions

were placed in the spectrophotometer (path length 1 cm), and heated or cooled at a rate of 0.2 °C min^{-1}. The absorptions of the solution at $\lambda = 500$ nm were recorded every 5 s. The cloud point temperature (T_{cp}) was determined as the one at which the transmittance at $\lambda = 500$ nm had reached 50% of the value difference between the initial and final stages. Circular dichroism (CD) measurements were performed on a JASCO J-815 spectropolarimeter with a thermocontrolled 0.2 mm quartz cell (five accumulations; "continues scanning" mode; scanning speed: 100 nm min^{-1}; data pitch: 0.5 nm; response: 1 s; bandwidth: 2.0 nm).

Synthesis of Et-OEG

Pyridinium chlorochromate (0.51 g, 2.37 mmol) was added to a solution of ethoxyl-terminated first-generation OEG-based dendritic alcohols (1.00 g, 1.57 mmol) in DCM (20 mL) at 0 °C, and then the reaction temperature was elevated to room temperature. After stirring for 3 h, the solvent was evaporated under vacuum, and the residue was purified twice by column chromatography (DCM/MeOH, 40:1 v/v) to afford **Et-OEG** (0.80 g, 80%) as a colorless oil.

^{1}H NMR ($CDCl_3$): $\delta = 1.19$–1.22 (t, 9H, CH_3), 3.51–3.89 (m, 36H, CH_2), 4.21–4.28 (m, 6H, CH_2), 7.14 (s, 2H, CH), 9.82 (s, 1H, CHO). HR-MS: m/z calcd for $C_{31}H_{54}O_{13}Na$ $[M + Na]^+$ 657.3462; found 657.3454.

Synthesis of Me-OEG

Pyridinium chlorochromate (1.10 g, 5.10 mmol) was added to a solution of methoxyl-terminated first-generation OEG-based dendritic alcohols (2.03 g, 3.41 mmol) in DCM (60 mL) at 0 °C, and then the reaction temperature was elevated to room temperature. After stirring for 3 h, the solvent was evaporated under vacuum, and the residue was purified twice by column chromatography (DCM/MeOH, 40:1 v/v) to afford **Me-OEG** (1.60 g, 79%) as a colorless oil.

^{1}H NMR ($CDCl_3$): $\delta = 3.37$ (m, 9H, CH_3), 3.51–3.89 (m, 30H, CH_2), 4.21–4.28 (m, 6H, CH_2), 7.14 (s, 2H, CH), 9.82 (s, 1H, CHO). HR-MS: m/z calcd for $C_{28}H_{48}O_{13}Na$ $[M + Na]^+$ 615.2993; found 615.2988.

Synthesis of Et-NP

Excess of $NaBH_4$ (200 mM) was added to the solution of **Et-P** (3 mM) in pH = 11 buffer at room temperature. After stirring overnight, the **Et-NP** with around 56% OEG coverage was yielded, which was purified with dialysis against deionized water. This reduction reaction was verified by ^{1}H NMR spectra (Supporting Information Fig. S1). After the addition of $NaBH_4$, the proton signals from **Et-OEG** and **Et-P** disappeared, while some new proton signals corresponding to dendritic alcohols **Et-OEG-OH** and **Et-NP** emerged. This demonstrates that **Et-P** was totally reduced to form nondynamic **Et-NP**.

RESULTS AND DISCUSSION

Imine Formation at Room Temperature

The formation of dynamic covalent polypeptides was conducted through mixing **PLL** with dendritic OEGs in aqueous solutions, which was verified with ^{1}H NMR spectroscopy [Fig. 2(a,b)]. Upon addition of 1 eq of **PLL** (based on the amino moieties) to the buffer solution of **Et-OEG** at pH = 11, the resolved proton signals (peaks 1 and 2) from monomeric **Et-OEG** at $\delta = 9.70$ and 7.26 ppm remained but their intensities significantly reduced. At the same time, new broad proton signals appeared at $\delta = 7.93$ and 6.84 ppm, which correspond to the imine and benzoic moieties from the polypeptide, respectively. The intensity reduction of the proton signals from **Et-OEG** and appearance of new broad signals prove that dendritic OEG units were attached onto **PLL** through the amine/aldehyde condensation to form the OEGylated polypeptide **Et-P**. The coexistence of **Et-P** and **Et-OEG** suggests thermodynamic equilibrium for the imine formation. By comparing the benzoic signal intensity from **Et-P** at $\delta = 6.84$ ppm with that from **Et-OEG** at $\delta = 7.26$ ppm, the imine yield was calculated to be about 59.0%. Similarly, the more hydrophilic polymeric imine **Me-P** was formed by mixing equivalent **PLL** and **Me-OEG** with a yield around 50.9% (Supporting Information Fig. S2). For comparison, monomeric imines **Et-M** and **Me-M** were prepared by reactions of pentylamine with **Et-OEG** and **Me-OEG**, respectively, to verify possible polymeric effects on the imine formation. ^{1}H NMR spectrum of the reaction mixture for **Et-OEG** is shown in Figure 2(c). The well-resolved new-born proton signals at $\delta = 8.15$ and 7.06 ppm correspond to imine and benzoic moieties from the monomeric imine **Et-M**, respectively. By counting the intensity ratio of benzoic signal at 7.06 ppm from **Et-M** with that at 7.26 ppm from **Et-OEG**, the imine yield was calculated to be 22.0%, which is much lower than that in polymeric imines **Et-P** and **Me-P**. The enhancement of imine formation with **PLL** could be mainly ascribed to local concentration enrichment of amino moieties along **PLL** chains. Certainly, pK_a decrease of amino moieties in **PLL** when compared with pentylamine should be another reason to contribute partially to the enhancement.[7(a)]

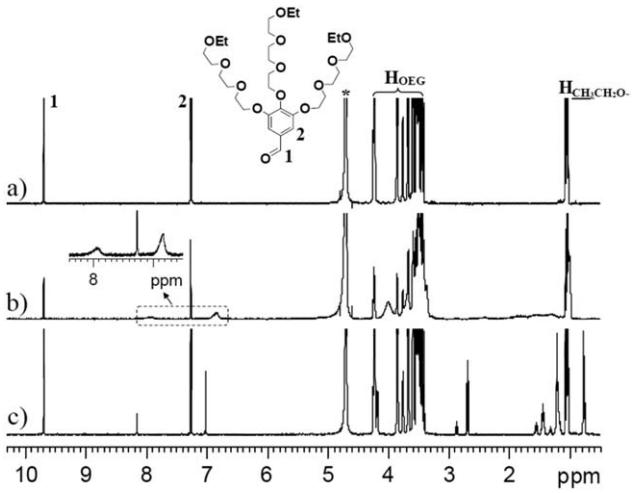

FIGURE 2 ^{1}H NMR spectra of **Et-OEG** (a), an equivalent mixture of **Et-OEG** and **PLL** (b), and an equivalent mixture of **Et-OEG** and pentylamine (c) in pH = 11 buffer at room temperature. [**Et-OEG**] = 3 mM.

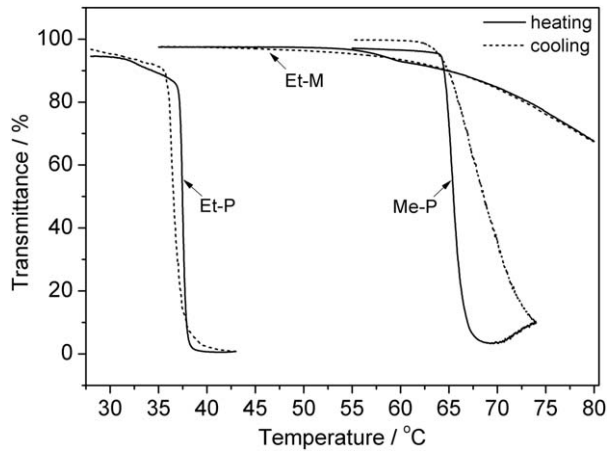

FIGURE 3 Plots of transmittance versus temperature for **Et-P**, **Me-P**, and **Et-M** in pH = 11 buffer. [c] = 3 mM.

Thermoresponsive Properties

The dendritic OEGs or **PLL** alone are not thermoresponsive even up to 80 °C. In contrast, the formed OEGylated polypeptides (**Et-P** and **Me-P**) are water soluble at room temperature, but exhibit typical thermoresponsive behavior at elevated temperature. Therefore, their thermally induced phase transition processes were followed by using UV/vis spectroscopy, and the typical turbidity curves are shown in Figure 3. Both OEGylated polypeptides show quite fast and sharp phase transitions during heating ($\Delta < 2$ K). For hydrophobic **Et-P** a very small hysteresis ($\Delta < 1$ K) was observed, but hydrophilic **Me-P** showed an abnormal reversible behavior during the cooling process, which is caused by thermally induced precipitation. The cloud point temperatures (T_{cp}) for **Et-P** and **Me-P** were determined to be 37.5 and 65.5 °C, respectively. This large difference of T_{cp}s indicates their high dependence on terminal groups of OEG moieties. Although OEG dendron coverage on **PLL** chains is relatively low at the given conditions (50–59%), these polypeptides adopt similar thermoresponsive behavior as the covalent OEGylated dendronized polymethacrylates (OEG coverage = 100%)[25] in both phase transition behavior and transition temperatures. These suggest that polypeptides could be endowed with superior thermoresponsiveness when reasonable amount of OEG units are attached onto their side chains. For comparison, thermoresponsiveness of monomeric imines (**Me-M** and **Et-M**) was also examined. Ethoxyl-terminated **Et-M** is thermoresponsive but its T_{cp} is higher than 70 °C. Furthermore, its phase transition is quite broad (>20 K). Methoxyl-terminated **Me-M** is too hydrophilic to show any thermoresponsiveness even at very high temperature (90 °C). The significant difference in thermoresponsive properties between polymeric and monomeric imines can be ascribed to the macromolecular effect, which facilitates both formation of the imines and the thermally induced collapse and aggregation kinetics of neighboring dendrons.

As imine bonds in aqueous solutions are dynamic in nature,[26] the coverage of dendritic OEG on **PLL** chains through imine linkage will change with external conditions, such as concentration and pH, which may lead to different expression of thermoresponsiveness for the OEGylated **PLL**s. Herein, these two external conditions were modulated independently to examine the effects of OEG coverage on the thermoresponsive behavior, and **Et-P** was selected as a representative. The plots of its T_{cp} and OEG coverage (x)[27] versus concentration or pH are shown in Figure 4 (for corresponding turbidity curves, see Supporting Information Fig. S5). When the concentration of **Et-P** decreased from 3 to 0.5 mM (at pH = 11), x reduced significantly from 59.0 to 6.8%. At the same time, T_{cp} increased dramatically from 37.5 to 53.3 °C ($\Delta = 15.8$ K), and the phase transition became broad simultaneously together with the appearance of obvious hysteresis. On the other hand, a decrease of pH from 11 to 9 also led to a large decrease of x, which causes a steep increase of T_{cp} ($\Delta = 23.9$ K) and broadening of phase transitions. Certainly, reduction of pH values also leads to enhanced protonation of amino groups as well as helicity decrease of polypeptide, which should also contribute to the increase of T_{cp} and broadness of phase transitions.[28] These results demonstrate that thermoresponsiveness of the dynamic OEGylated polypeptides is closely related to coverage of the dendritic OEG along PLL chains. Coverage decrease leads to the higher T_{cp}, broader phase transition, as well as larger hysteresis. To verify effects of imine dynamic

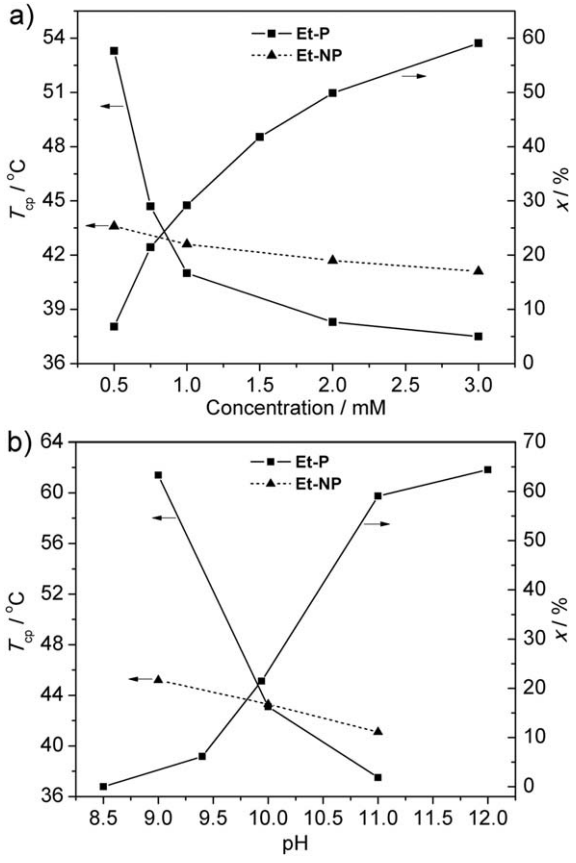

FIGURE 4 Plots of T_{cp} and x versus concentration (fixed pH = 11) (a) and pH (fixed [c] = 3 mM) (b) for both **Et-P** and **Et-NP**.

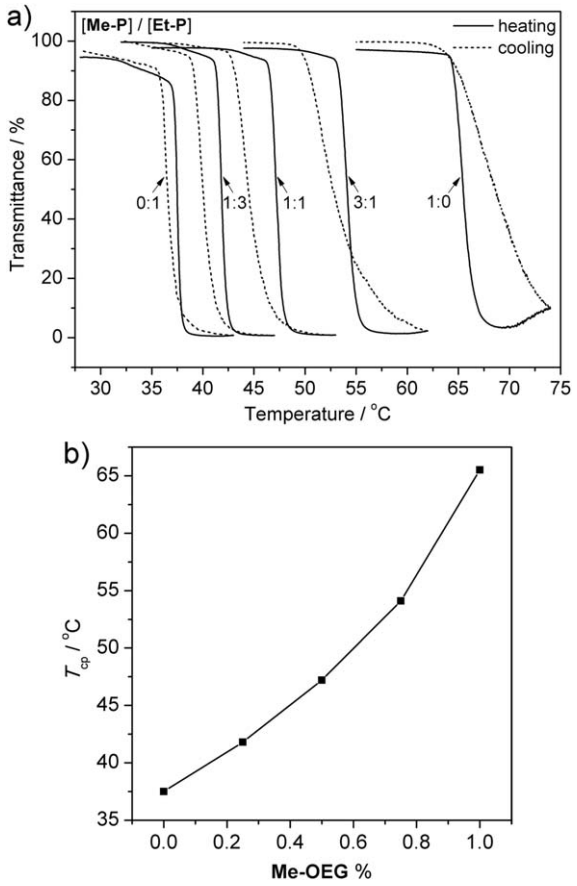

FIGURE 5 (a) Plots of transmittance versus temperature for the mixture of **Me-P** and **Et-P** at different mole ratios (0:1, 1:3, 1:1, 3:1, and 1:0) in pH = 11 buffer. (b) Plot of T_{cp} against the mole ratio of **Me-OEG**. [c] = 3 mM.

nature on the thermoresponsive behavior, **Et-P** was reduced with $NaBH_4$ to form the corresponding nondynamic polypeptide **Et-NP**. This nondynamic polypeptide possesses an OEG coverage around 56%, and its thermoresponsiveness was investigated (for turbidity curves, see Supporting Information Fig. S6). The T_{cp} of **Et-NP** increased slightly from 41.1 to 43.6 °C ($\Delta = 2.5$ K) when the concentration was decreased from 3 to 0.5 mM, while it reduced moderately from 45.2 to 41.1 °C ($\Delta = 4.1$ K) when solution pH was changed from 9.0 to 11.0. These small variations make sharp contrast to the case of dynamic **Et-P**, indicating that dynamic imine linkage plays a key role in mediating thermoresponsiveness of the polypeptides.

Based on reversibility of the dynamic imine linkage in OEGylated polypeptides, it should be possible to tune the overall hydrophilicity–hydrophobicity balance through imine exchange, and this can be done by using dendritic OEGs of different hydrophilicity. Through mixing homopolypeptides **Et-P** and **Me-P** at different mole ratios, the random copolypeptides would be formed via the imine exchange based on similar reactivities of **Me-OEG** and **Et-OEG** toward **PLL**. In the same way as the parent homopolypeptides, these copolypeptides show quite fast phase transitions and small hysteresis [Fig. 5(a)]. Their T_{cp}s are completely dependent on the mole ratios of two homopolypeptides [Fig. 5(b)], and were determined to be 41.8, 47.2, and 54.1 °C for the mole ratios of **Me-P**/**Et-P** at 1:3, 1:1, and 3:1, respectively. These results indicate that the phase transition temperatures of the dynamic OEGylated polypeptides are fully tunable in the range of 37–66 °C simply through adjusting mole ratios of two dendritic OEGs with different hydrophilicities.

Effects of Thermally Induced Phase Transitions on Imine Linkage

Temperature-varied ^{1}H NMR spectroscopy was used to examine the effect of thermally induced phase transitions on the dynamic imine linkage. The monomeric imine **Et-M** was selected as the representative because its proton signals are well resolved when compared to its polymeric counterpart. For comparison, the nonthermoresponsive **Me-M** was also checked. Typical ^{1}H NMR spectra of **Et-M** formed from equivalent **Et-OEG** and pentylamine in the range of $\delta = 7.9$–10.9 ppm from 30 to 70 °C are shown in Figure 6(a) (for full spectra, see Supporting Information Fig. S7). Below the phase transition temperature, the proton signals from **Et-M** and **Et-OEG** coexist and remain in single group. As the temperature increases to 46 °C which is right below the aggregation point (46.7 °C), proton signals from **Et-M** split into two groups (peaks 3, 3′, 4, and 4′), while those from **Et-OEG** remain one group (peaks 1 and 2). Proton splitting for **Et-M** suggests that OEG collapse from water renders **Et-M** into two physicochemical states, which possesses a slow exchange process on the NMR timescale. The downfield signals (3, 4) correspond to **Et-M** in hydrated state, and the upfield (3′, 4′) to **Et-M** in dehydrated state. With further increase of solution temperature, the content of dehydrated imine increases gradually, while the content of hydrated imine decreases. By comparing these signal intensities, the yield of **Et-M** (both in hydrated and dehydrated states) can be calculated, and the results are plotted in Figure 6(b). As expected, the yield of **Et-M** decreases linearly with the increase of temperature below T_{cp}. However, as the temperature increases above T_{cp}, the yield increases abruptly. This tendency is enhanced with the further increase of solution temperature, and the imine yield reaches 35.6% at 70 °C, which is even slightly higher than that (28.1%) at 23 °C, indicating that thermally induced aggregation facilitates the imine formation in the case of **Et-M**. For comparison, the yield of hydrophilic **Me-M** was also followed, which is found to be decreased continuously during the whole heating process [Fig. 6(b)]. Above results demonstrate that the thermally induced phase transition can effectively promote the formation of imine in aqueous solutions even at high temperatures, providing that the collapsed phase is hydrophobic enough. Enhancement of imine formation in thermally induced aggregation of **Et-M** was further verified by mixing **Et-M** with a thermoresponsive covalent dendronized polymer **Et-PG1** (for its molecular structure, see Supporting Information Fig. S8)[25(b)] at different temperatures. The addition of **Et-PG1** into the mixture of **Et-OEG** and pentylamine shows negligible influence on the yield of **Et-M** at room

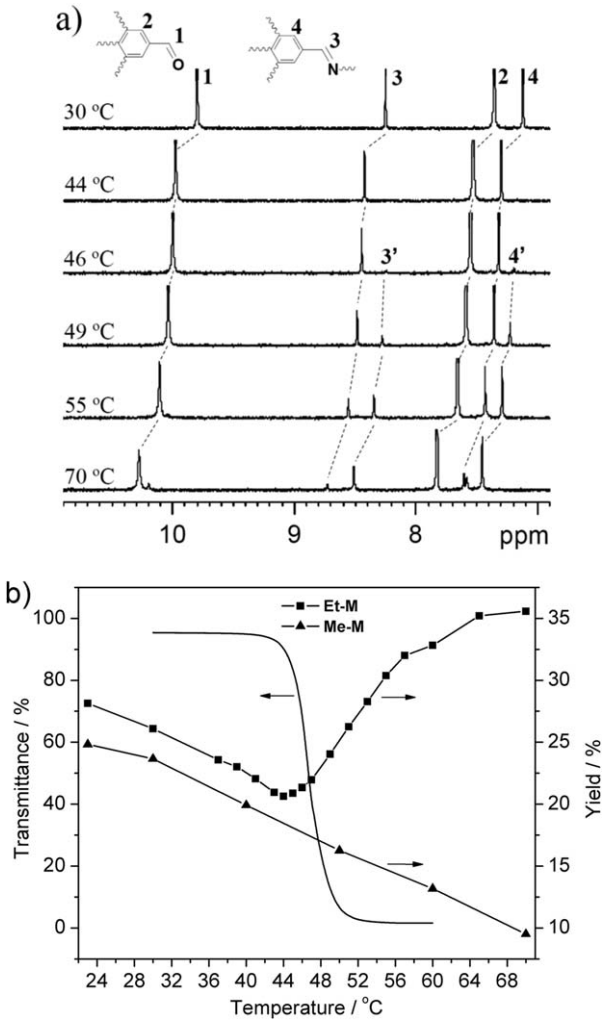

FIGURE 6 (a) Temperature-varied ^{1}H NMR spectra of **Et-M** in buffer. (b) Plots of transmittance and imine yield versus temperature for **Et-M** in buffer. The imine yield for **Me-M** on the temperature is also included. pH = 11, [c] = 5 mM.

temperature (Supporting Information Fig. S9). However, as the temperature increased to 32 °C, which is right around the phase transition temperature of **Et-PG1** but far below that of **Et-M**, the proton signals from **Et-M** split into two groups, suggesting that **Et-M** was partially encapsulated in the hydrophobic domain formed by the dehydration and aggregation of **Et-PG1**. As a result, the yield of **Et-M** increases obviously from 26.7 to 39.1% when temperature increases from 30 to 49 °C. Hence, the dehydration and collapse of OEG units from the water could provide a unique hydrophobic microenvironment, which effectively facilitates imine formation and inhibits to some extent imine hydrolysis in aqueous solutions. Similar enhancement of imine formation in aqueous conditions was also observed in other amphiphilic self-assembly systems.[29]

Secondary Structures of the OEGylated Polypeptides

Secondary structures of these OEGylated polypeptides were investigated by CD spectroscopy. To examine possible effect of dynamic OEGylation on the secondary structures, **PLL**s with different OEG coverage were prepared by changing the mole ratio of **Et-OEG** to amino moieties from **PLL** ([**Et-OEG**]/[$\mathbf{NH_2}$]), and their CD spectra are shown in Figure 7(a). At pH = 11, the native **PLL** adopts a typical α-helical conformation at room temperature as indicated by Cotton effects with a maximum at $\lambda = 191$ nm and two minima at $\lambda = 208$ and 222 nm. Upon successive addition of **Et-OEG**, OEG coverage on polypeptide chains increased gradually, and the mean residual molar ellipticity at $\lambda = 222$ nm ($[\theta]_{222}$) increased accordingly [Fig. 7(b)]. When [**Et-OEG**]/[$\mathbf{NH_2}$] reached 0.5, $[\theta]_{222}$ tends to reach a maximum value of about 35,000° cm^2 dmol^{-1}, corresponding to nearly 100% helicity.[30] Similar helical conformation enhancement was also observed at pH = 10 where a relatively low OEG coverage (21.4%) was reached (Supporting Information Fig. S10). This demonstrates that attachment of OEG units onto **PLL** chains could effectively enhance the polypeptide helicity, which should result from shielding of static or charge repulsion among residual amino pendants through OEG dendrons.

Based on their unique thermoresponsiveness, influence of temperature on the secondary structures of these OEGylated

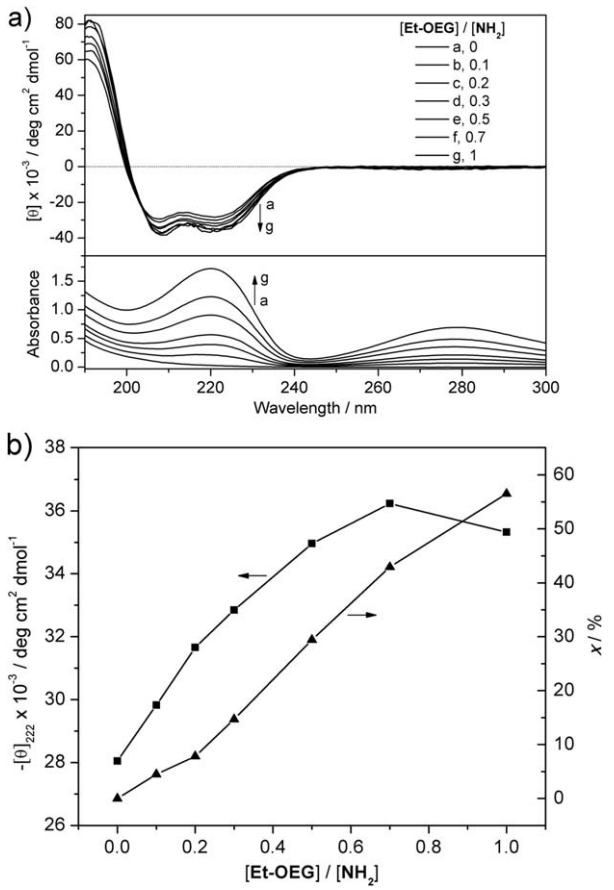

FIGURE 7 (a) CD spectra of **PLL** in pH = 11 buffer ([$\mathbf{NH_2}$] = 3 mM) with different amounts of **Et-OEG**. [**Et-OEG**]/[$\mathbf{NH_2}$] represents the mole ratio of **Et-OEG** to lysine units in **PLL**. (b) Plot of $-[\theta]_{222}$ and x against [**Et-OEG**]/[$\mathbf{NH_2}$].

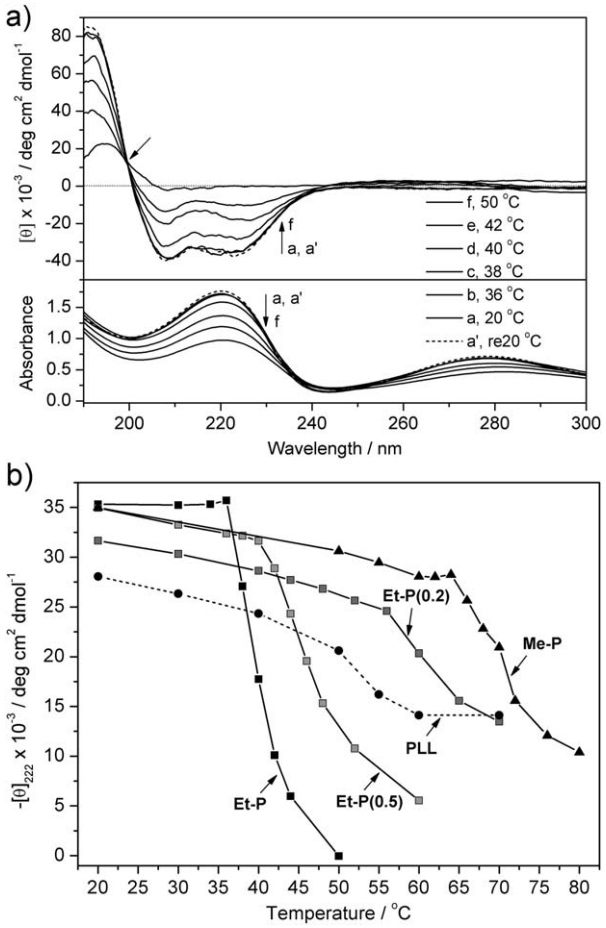

FIGURE 8 (a) Temperature-varied CD spectra of **Et-P** in pH = 11 buffer. (b) Plots of $[\theta]_{222}$ versus temperature for **Et-P**, **Me-P**, **Et-P(0.5)**, and **Et-P(0.2)** in pH = 11 buffer. **Et-P(0.5)** and **Et-P(0.2)** represent these formed with [**Et-OEG**]/[$\mathbf{NH_2}$] ratios to be 0.5 and 0.2, respectively. [$\mathbf{NH_2}$] = 3 mM.

polypeptides was examined, and resulting CD spectra from **Et-P** are plotted in Figure 8(a). Below the phase transition temperature, $[\theta]_{222}$ remains nearly the same at about 35,000° cm^2 $dmol^{-1}$ with increase of temperature. However, as temperature reached 38 °C which is around the phase transition point (37.5 °C), $[\theta]_{222}$ reduced greatly to 27,000° cm^2 $dmol^{-1}$, indicating that the ordered conformation of polypeptide was disrupted partially upon chain collapse from water. With further elevation of solution temperature, $[\theta]_{222}$ decreased continuously, and nearly down to zero at 50 °C. Once the solution was cooled down to room temperature, the ordered secondary structures of **Et-P** recovered completely [compare curves a with a′ in Fig. 8(a)]. Notably, the presence of an isosbestic point at around $\lambda = 200$ nm (marked with an arrow) suggests that polypeptide conformation was exclusively transformed between ordered α-helix and disordered random conformation during the thermally induced aggregation process. Similar phenomena were also observed for the more hydrophilic **Me-P** [Fig. 8(b), for CD spectra, see Supporting Information Fig. S11], but its $[\theta]_{222}$ decreased evidently at around 66 °C (its T_{cp}) which is far above the crucial turn point for **Et-P**. To further illustrate the effects of thermally induced collapse and aggregation on the secondary structure transitions of polypeptides, **PLL**s with different OEG coverage **Et-P(0.5)** and **Et-P(0.2)** were prepared by changing the ratios of [**Et-OEG**]/[$\mathbf{NH_2}$] to be 0.5 and 0.2, respectively. Their $[\theta]_{222}$ versus temperature is plotted in Figure 8(b) (for CD spectra, see Supporting Information Fig. S12). For the native **PLL**, $[\theta]_{222}$ decreased slowly with increase of temperature from 20 to 60 °C, and tended to be unchanged at 60 °C as a result of the α-helix-to-β-sheet transition. However, the OEGylated polypeptide **Et-P** with a high OEG coverage (59.0%) underwent great drop of $[\theta]_{222}$ at the onset of the phase transition (38 °C), and decreased sharply with increase of temperature. When OEG coverage was reduced to around 29.4% in the case of **Et-P(0.5)**, this OEGylated polypeptide showed similar thermoresponsive behavior as **Et-P**, except an increased T_{cp} (41.8 °C) together with a slightly broader phase transition and larger hysteresis (for turbidity curves, see Supporting Information Fig. S13). As a result, its $[\theta]_{222}$ reduced evidently at around 42 °C, and the decrease was less sharper than that of **Et-P** with increase of temperature. When OEG coverage was further decreased to around 7.8% for the case of **Et-P(0.2)**, its phase transition became very broad, and $[\theta]_{222}$ showed much slower decrease during the heating process, which resembles very much as the native **PLL**. Above results demonstrate that helicity of OEGylated polypeptides was destroyed significantly once the solution temperature increased above their cloud point temperatures. The tendency for their helicity decrease during phase transitions was dominated by OEG coverage: the larger the OEG coverage, the more significant the decrease of helicity. This suggests that the collapse and aggregation of dendritic OEG side chains could probably weaken the intramolecular hydrogen bonding of polypeptide backbone, which is the main driving force for the formation of stable α-helical conformation. The higher OEG coverage around the polypeptide chains could lead to the formation of larger crowdedness and solubility to prohibit intramolecular hydrogen bonding, thus forming more disorder conformation. Certainly, steric hindrance from collapsed OEG units may also contribute to diminishing the ordered structures. Therefore, through finely tuning OEG coverage, secondary structures of these OEGylated polypeptides can be reversibly switched to be ordered or disordered based on their thermoresponsiveness.

CONCLUSIONS

In summary, we have presented a novel strategy for endowing polypeptides simultaneously with tunable thermoresponsive properties and secondary structures through DCC. These polypeptides were formed through the reversible imine condensation between poly(L-lysine)s and dendritic OEG motifs in aqueous solutions. Besides the contributions from solution concentrations, pH values, component ratios, as well as hydrophobicity of the components, the imine formation can be enhanced significantly when reactions are performed on macromolecules. Thermoresponsiveness of these OEGylated

polypeptides is dominated by terminal groups and coverage of OEG dendrons. Thanks to the dynamic feature from imines, their phase transition temperatures can be easily tuned through imine exchange between dendritic OEGs of different hydrophilicity. Secondary structures of these OEGylated polypeptides are dependent on OEG coverage, and can be tuned through thermally induced aggregation. Attached OEG dendrons along polypeptide backbone provide shielding effects to obviously enhance α-helical conformation. Thermally induced aggregation can promote the imine formation in aqueous environment when the reactants are hydrophobic enough and, at the same time, distort the ordered secondary structures probably due to the diminished intramolecular hydrogen bonding. Based on the dynamic characteristics of imine linkage, it is convenient to tune the thermoresponsive properties and secondary structures of these OEGylated polypeptides. Considering the excellent biocompatibility of OEGylated polymers, these novel stimuli-responsive polypeptides would find promising applications in bio-related functional materials. We thus expect that the novel strategy developed in this work could inspire the exploration of novel stimuli-responsive (poly)peptides to extend their applications in biological and biomedical systems.

ACKNOWLEDGMENTS

The authors sincerely thank Toshio Masuda for his help in corrections of the manuscript. Hongmei Deng from the Instrumental Analysis and Research Center of Shanghai University is thanked for her assistance with the NMR measurements. They thank the National Natural Science Foundation of China (Nos. 21034004, 21104043, 21374058, and 21304056), the Ph.D. Programs Foundation of Ministry of Education of China (Nos. 201131081200177 and 201331081100166), and the Shanghai Postdoctoral Sustentation Fund (No. 13R21413200) for their financial supports.

REFERENCES AND NOTES

1 (a) C. M. Dobson, *Nature* (**2003**), *426*, 884–890; (b) T. J. Deming, *Prog. Polym. Sci.* (**2007**), *32*, 858–875; (c) M. Zelzer, R. V. Ulijn, *Chem. Soc. Rev.* (**2010**), *39*, 3351–3357; (d) C. Deng, J. Wu, R. Cheng, F. Meng, H.-A. Klok, Z. Zhong, *Prog. Polym. Sci.* (**2014**), *39*, 330–364.

2 (a) M. Goodman, A. S. Verdini, C. Toniolo, W. D. Phillips, F. A. Bovey, *Proc. Natl. Acad. Sci. U.S.A.* (**1969**), *64*, 444–450; (b) R. V. Ulijn, A. M. Smith, *Chem. Soc. Rev.* (**2008**), *37*, 664–675; (c) W. Li, X. Zhang, J. Wang, X. Qiao, K. Liu, A. Zhang, *J. Polym. Sci. Part A: Polym. Chem.* (**2012**), *50*, 4063–4072; (d) X. Chang, C.-M. Dong, *Biomacromolecules* (**2013**), *14*, 3329–3337; (e) S. H. Wibowo, E. H. H. Wong, A. Sulistio, S. N. Guntari, A. Blencowe, F. Caruso, G. G. Qiao, *Adv. Mater.* (**2013**), *25*, 4619–4624.

3 F. Zhang, O. Sadovski, S. J. Xin, G. A. Woolley, *J. Am. Chem. Soc.* (**2007**), *129*, 14154–14155.

4 A. Patgiri, A. L. Jochim, P. S. Arora, *Acc. Chem. Res.* (**2008**), *41*, 1289–1300.

5 F. Ruan, Y. Chen, P. B. Hopkins, *J. Am. Chem. Soc.* (**1990**), *112*, 9403–9404.

6 S. Marqusee, R. L. Baldwin, *Proc. Natl. Acad. Sci. U.S.A.* (**1987**), *84*, 8898–8902.

7 (a) A. Harada, S. Cammas, K. Kataoka, *Macromolecules* (**1996**), *29*, 6183–6188; (b) Y. Lim, K.-S. Moon, M. Lee, *Angew. Chem. Int. Ed.* (**2009**), *48*, 1601–1605.

8 (a) H. Lu, J. Wang, Y. Bai, J. W. Lang, S. Liu, Y. Lin, J. Cheng, *Nat. Commun.* (**2011**), *2*, 206; (b) Y. Zhang, H. Lu, Y. Lin, J. Cheng, *Macromolecules* (**2011**), *44*, 6641–6644.

9 (a) S. Zhang, Z. Li, *J. Polym. Sci. Part B: Polym. Phys.* (**2013**), *51*, 546–555; (b) J. Huang, A. Heise, *Chem. Soc. Rev.* (**2013**), *42*, 7373–7390.

10 K.-S. Krannig, H. Schlaad, *J. Am. Chem. Soc.* (**2012**), *134*, 18542–18545.

11 (a) J. R. Kramer, T. J. Deming, *J. Am. Chem. Soc.* (**2012**), *134*, 4112–4115; (b) J. R. Kramer, T. J. Deming, *J. Am. Chem. Soc.* (**2014**), *136*, 5547–5550.

12 K. Pagel, B. Koksch, *Curr. Opin. Chem. Biol.* (**2008**), *12*, 730–739.

13 D. W. P. M. Löwik, E. H. P. Leunissen, M. van den Heuvel, M. B. Hansen, J. C. M. van Hest, *Chem. Soc. Rev.* (**2010**), *39*, 3394–3412.

14 (a) W. F. Daamen, J. H. Veerkamp, J. C. M. van Hest, T. H. van Kuppevelt, *Biomaterials* (**2007**), *28*, 4378–4398; (b) A. J. Simnick, D. W. Lim, D. Chow, A. Chilkoti, *Polym. Rev.* (**2007**), *47*, 121–154; (c) H. Nuhn, H.-A. Klok, *Biomacromolecules* (**2008**), *9*, 2755–2763.

15 (a) F. Chen, X. Zhang, W. Li, K. Liu, Y. Guo, J. Yan, A. Zhang, *Soft Matter* (**2012**), *8*, 4869–4872; (b) C. M. Chopko, E. L. Lowden, A. C. Engler, L. G. Griffith, P. T. Hammond, *ACS Macro Lett.* (**2012**), *1*, 727–731.

16 (a) M. Yu, A. P. Nowak, T. J. Deming, *J. Am. Chem. Soc.* (**1999**), *121*, 12210–12211; (b) Y. Cheng, C. He, C. Xiao, J. Ding, X. Zhuang, X. Chen, *Polym. Chem.* (**2011**), *2*, 2627–2634; (c) C. Chen, Z. Wang, Z. Li, *Biomacromolecules* (**2011**), *12*, 2859–2863; (d) Y. Liao, C.-M. Dong, *J. Polym. Sci. Part A: Polym. Chem.* (**2012**), *50*, 1834–1843; (e) X. Fu, Y. Shen, W. Fu, Z. Li, *Macromolecules* (**2013**), *46*, 3753–3760.

17 X. Zhang, W. Li, X. Zhao, A. Zhang, *Macromol. Rapid Commun.* (**2013**), *34*, 1701–1707.

18 (a) S. J. Rowan, S. J. Cantrill, G. R. L. Cousins, J. K. M. Sanders, J. F. Stoddart, *Angew. Chem. Int. Ed.* (**2002**), *41*, 898–952; (b) J.-M. Lehn, *Chem. Soc. Rev.* (**2007**), *36*, 151–160; (c) R. J. Wojtecki, M. A. Meador, S. J. Rowan, *Nat. Mater.* (**2011**), *10*, 14–27; (d) E. Moulin, G. Cormos, N. Giuseppone, *Chem. Soc. Rev.* (**2012**), *41*, 1031–1049.

19 (a) P. T. Corbett, J. Leclaire, L. Vial, K. R. West, J.-L. Wietor, J. K. M. Sanders, S. Otto, *Chem. Rev.* (**2006**), *106*, 3652–3711; (b) T. Maeda, H. Otsuka, A. Takahara, *Prog. Polym. Sci.* (**2009**), *34*, 581–604; (c) Y. Jin, C. Yu, R. J. Denman, W. Zhang, *Chem. Soc. Rev.* (**2013**), *42*, 6634–6654; (d) D. Wang, H. Chen, Y. Su, F. Qiu, L. Zhu, X. Huan, B. Zhu, D. Yan, F. Guo, X. Zhu, *Polym. Chem.* (**2013**), *4*, 85–94.

20 R. T. S. Lam, A. Belenguer, S. L. Roberts, C. Naumann, T. Jarrosson, S. Otto, J. K. M. Sanders, *Science* (**2005**), *308*, 667–669.

21 J. M. A. Carnall, C. A. Waudby, A. M. Belenguer, M. C. A. Stuart, J. J.-P. Peyralans, S. Otto, *Science* (**2010**), *327*, 1502–1506.

22 (a) J. W. Sadownik, R. V. Ulijn, *Curr. Opin. Biotechnol.* (**2010**), *21*, 401–411; (b) J. Li, P. Nowak, S. Otto, *J. Am. Chem. Soc.* (**2013**), *135*, 9222–9239; (c) C. Wang, G. Wang, Z. Wang, X. Zhang, *Chem. Eur. J.* (**2011**), *17*, 3322–3325; (d) A. K. H. Hirsch, E. Buhler, J.-M. Lehn, *J. Am. Chem. Soc.* (**2012**), *134*, 4177–4183.

23 Actually, dynamic covalent chemistry has been extensively applied to mediate thermoresponsive polymers with tunable properties, for example see: (a) B. S. Murray, A. W. Jackson, C. S. Mahon, D. A. Fulton, *Chem. Commun.* (**2010**), *46*, 8651–8653; (b) D. E. Whitaker, C. S. Mahon, D. A. Fulton, *Angew. Chem. Int. Ed.* (**2013**), *52*, 956–959; (c) A. W. Jackson, D. A. Fulton, *Polym. Chem.* (**2013**), *4*, 31–45; (d) J. Li, S. Yang, L. Wang, X. Wang, L. Liu, *Macromolecules* (**2013**), *46*, 6832–6842.

24 (a) C. M. Haney, M. T. Loch, W. S. Horne, *Chem. Commun.* (**2011**), *47*, 10915–10917; (b) C. M. Haney, W. S. Horne, *Chem. Eur. J.* (**2013**), *19*, 11342–11351.

25 (a) W. Li, A. Zhang, K. Feldman, P. Walde, A. D. Schlüter, *Macromolecules* (**2008**), *41*, 3659–3667; (b) W. Li, A. Zhang, A. D. Schlüter, *Chem. Commun.* (**2008**), *5523*-5525; (c) W. Li, D. Wu, A. D. Schlüter, A. Zhang, *J. Polym. Sci. Part A: Polym. Chem.* (**2009**), *47*, 6630–6640; (d) M. J. N. Junk, W. Li, A. D. Schlüter, G. Wegner, H. W. Spiess, A. Zhang, D. Hinderberger, *Angew. Chem. Int. Ed.* (**2010**), *49*, 5683–5687; (e) J. Yan, X. Zhang, W. Li, X. Zhang, K. Liu, P. Wu, A. Zhang, *Soft Matter* (**2012**), *8*, 6371–6377; (f) J. Yan, W. Li, A. Zhang, *Chem. Commun.* **2014**, *50*, 12221–12233.

26 (a) M. E. Belowich, J. F. Stoddart, *Chem. Soc. Rev.* (**2012**), *41*, 2003–2024; (b) Y. Xin, J. Yuan, *Polym. Chem.* (**2012**), *3*, 3045–3055.

27 All the values of x at different concentrations or pH were calculated by comparing the signal intensity of benzoic imine from **Et-P** at $\delta = 6.84$ ppm with that from **Et-OEG** at $\delta = 7.26$ ppm (see spectra in Supporting Information Figs. S3 and S4).

28 H. Feil, Y. H. Bae, J. Feijen, S. W. Kim, *Macromolecules* (**1993**), *26*, 2496–2500.

29 (a) R. Nguyen, L. Allouche, E. Buhler, N. Giuseppone, *Angew. Chem. Int. Ed.* (**2009**), *48*, 1093–1096; (b) D. Janeliunas, P. van Rijn, J. Boekhoven, C. B. Minkenberg, J. H. van Esch, R. Eelkema, *Angew. Chem. Int. Ed.* (**2013**), *52*, 1998–2001; (c) G. Wang, G. Wu, Z. Wang, X. Zhang, *Langmuir* (**2014**), *30*, 1531–1535.

30 J. A. Morrow, M. L. Segall, S. Lund-Katz, M. C. Phillips, M. Knapp, B. Rupp, K. H. Weisgraber, *Biochemistry* (**2000**), *39*, 11657–11666.